Two-Photon Polymerization 3D Printed Hydrophobic and Hydrophilic Surface Morphologies for Electrode Micropatterning via Dip Coating Techniques and Enhanced Microchannel Filling

*Stanislav Sikulskyi, Rishikesh Srinivasaraghavan Govindarajan, Taylor Stark, Zefu Ren, Nicholas Reed and Daewon Kim**

Dr. S. Sikulskyi, R. Srinivasaraghavan Govindarajan, T. Stark, Z. Ren, N. Reed, Dr. D. Kim
Department of Aerospace Engineering
Embry-Riddle Aeronautical University
1 Aerospace Blvd, Daytona Beach, FL 32114, USA
* Corresponding Author: kimd3c@erau.edu

Keywords: hydrophobic and hydrophilic, two-photon polymerization (2PP), additive manufacturing (AM), electrode micropatterning, microchannels

Abstract

Numerous existing and emerging microsize technologies operate by utilizing electrical circuits on surfaces and within solid objects, such as electrode micropatterns and filled microchannels. While current micropatterning techniques have achieved extensive performance of current systems through pattern resolution and discretization on surfaces with simple geometry, the introduction of many new applications relies on the complexity of parts on which these patterns are fabricated. Additionally, many state-of-the-art applications utilize novel materials for functional systems, which further complicates their fabrication. This paper introduces innovative electrode micropatterning and microchannel filling approaches that support complex three-dimensional designs and reduce the number of fabrication steps. The approaches leverage microsize hydrophobic and hydrophilic morphologies fabricated using the two-photon polymerization (2PP) additive manufacturing (AM) process, in conjunction with the target part. Once fabricated, the part is dipped into a conductive solution or another functional liquid, forming patterns on the surfaces and filling the channels based on the pre-designed wetting morphologies. These morphologies incorporate additional structures beyond the conventional hydrophilic and reentrant hydrophobic structures to facilitate the dipping process. This paper demonstrates the design of microstructures for a micropatterning approach that allows coating of electrodes using an electrode dipping process for the creation of a microsize strain gauge.

1. Introduction

The influence of surface morphology on its interaction with various media has been actively studied for several decades, drawing significant inspiration from nature.[1,2] Wetting is amongst the most attractive properties of surface morphologies due to its promising performance enhancement, introduction of new functionalities, and its myriad applications.[3,4] Specifically, hydrophobicity and hydrophilicity are properties of a surface to repel or attract water, respectively. Hydrophobic microstructures utilize a liquid's surface tension to suspend it above the surface, thereby minimizing the wetted surface area and, thus, reducing surface free energy. As such, so-called reentrant structures have garnered significant attention for the ability to suspend liquids with low contact angles on surface materials, and for other hydrophobic capabilities despite its manufacturing complexity.[5] In contrast, hydrophilic morphology enhances surface free energy by increasing wetted surface area. Consequently, a surface can drastically alter its behavior with liquids by manipulating the surface's morphology. Designing microstructures to control wettability, though not a novel concept, remains an actively studied phenomenon rooted in mimicking and replicating natural structures, like those found on the Phyllostachys aurea bamboo leaf.[6,7] Bio-inspired microstructures are frequently studied due to their reliability and the ease with which they can be compared to their natural counterparts. While there has been tremendous success in altering the wettability of flat surfaces through the addition of fabricated microstructures, many advanced applications could be developed and benefit

from the fabrication of wetting microstructures on complex surfaces that are variously oriented and curved.[8,9] However, manufacturing of complex high-performance microstructures is challenging. A variety of electrochemical techniques and processing procedures can be implemented, but lack precise control for application which is further complicated with intricate designs.[10-13] Additively manufacturing (AM) techniques, on the other hand, provide enhanced control over the application and customization of the targeted wettability microstructure. Furthermore, advancements in AM technologies enable the creation of micropatterns that have historically been difficult to manufacture on conformal surfaces and within microfluidic channels.

To introduce new capabilities through wetting morphologies on intricate parts, this paper implements two-photon polymerization (2PP) as a fabrication method. 2PP can produce complex micro-scale components along with their wetting morphologies in a single operation, drastically simplifying the fabrication process by enabling simultaneous fabrication of different microstructures on surfaces with high resolution (**Figure 1**a). Complex 2PP printed microstructures can attain sub-micrometer intricacies, allowing biomimetic microsize parts to be easily achievable.[14-23] Several designs have been printed, demonstrating hydrophobic and superhydrophobic functionality utilizing the 2PP technique.[14-19,23] Some designs leverage the inverse phenomena by attracting liquids rather than repelling them.[21] While having both hydrophobic and hydrophilic surfaces within itself is beneficial, their tandem use was shown to direct liquids into specific patterns or shapes with increased precision.[15,16,22]

After establishing the fabrication of wetting morphologies on complex geometries via 2PP, this paper introduces and enhances several promising applications. Firstly, wetting morphologies can be used for electrode micropatterning by selectively controlling surface wetting characteristics. Thus, 2PP printed structures with wetting morphologies can serve as a versatile fabrication technique for microscale electronics, sensors, and actuators, building upon the capabilities of previous efforts.[24-26] Primarily, after a part with hydrophobic and hydrophilic microstructures is 2PP printed, it can be dipped into a solution of conductive material to coat the selected areas, thereby creating arrays of conductive traces for distributed sensing and actuation capabilities. Following the dipping, the drying/curing process results in the final device with electrode pattern; however, this process must be performed meticulously to ensure proper electrode material deposition during evaporation.[27,28] Figure 1(b1 and c1) illustrates the fabrication of a microsize strain gage by dipping a 2PP printed part with wetting morphologies into a conductive solution, a process that is further designed and demonstrated in this paper. The designed dipping process fundamentally differs from most tests conducted with wetting microstructures, as the latter is mainly performed on horizontal surfaces. In contrast, known manufacturing methods that involve dipping often cater to parts with complex geometry that can be dipped in various orientations. Moreover, these parts are typically submerged in the solution fully rather than having individual droplets on the horizontal surface. This full immersion adds a hydrostatic pressure to the Laplace and perturbation pressure components. Consequently, the dipping process is studied to investigate solid-fluid interaction and design appropriate auxiliary microstructures enabling dipping complex parts with various patterns. In addition to hydrophobic structures preventing electrode coating on the unwanted areas, the effects of hydrophilic morphology in regions intended for electrode-coating are studied for the dipping process.

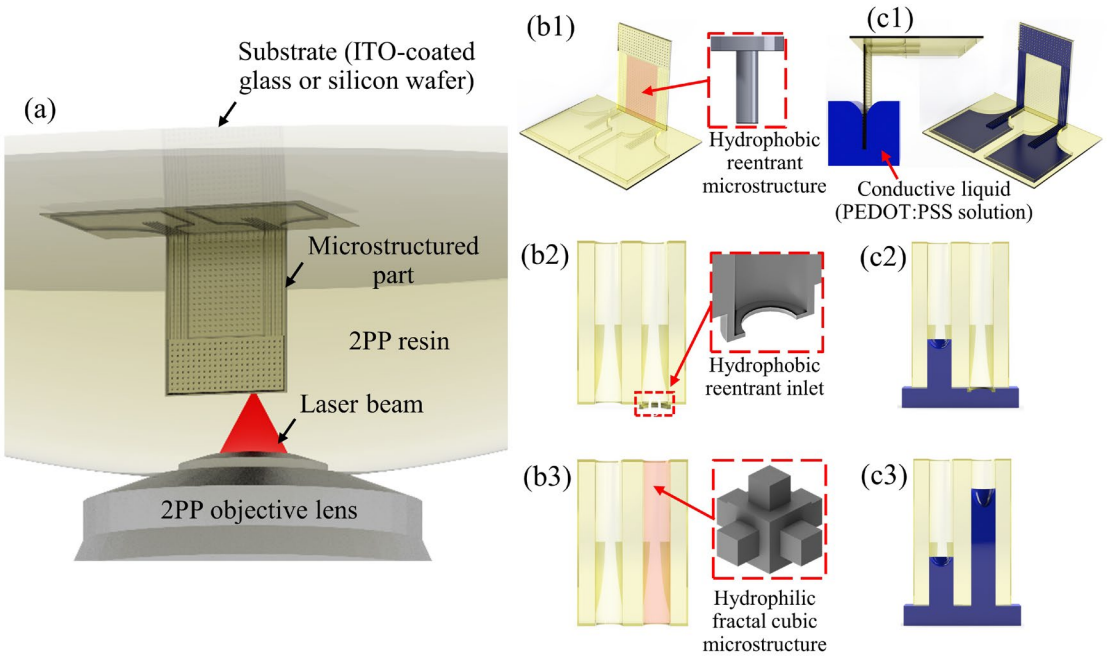

Figure 1. Visual summary of the paper depicting (a) 2PP additively manufacturing small-scale objects with (b1-b2) hydrophobic and (b3) hydrophilic microstructures resulting in (c1) technology of electrode micropatterning through dipping, (c2) selective microchannel filling or venting capability, and (c3) enhanced microchannel filling.

The second application developed in this study involves using 2PP printed parts with wetting morphologies for the selective and enhanced filling of microchannels, which are critical components of novel microfluidic devices.[29] Hydrophobic structures at the inlet of a microchannel can prevent a fluid from entering the channel until a specific pressure is applied, which depends on the hydrophobic structure design, the fluid's surface tension, and the contact angle on the microchannel material surface, as shown in Figure 1(b2 and c2). Utilizing this approach offers several capabilities, such as leaving the microchannel empty for venting and gas transfer or selective microchannel filling with different fluids. Specifically, if a microfluidic device has multiple channels that require selective filling with different fluids, a hydrophobic inlet can be designed to suspend one fluid while being wetted with another fluid. When the device is consequently dipped into two fluids in a control fashion, channels can be filled independently with different fluids, offering a range of potential functionalities, such as precise mixing, dosing, material synthesis, sensing, forming electrical circuits, and heat management.[30]

Regarding the enhancement of microchannel performance, microfluidics with hydrophilic structures have been proven viable.[11,31] However, fabricating microstructures inside a channel drastically limits manufacturing options and possible microstructure designs, typically leading to the use of multiple open molds with pre-fabricated microstructures on their surfaces and subsequent assembly of the molds.[32] As a result, such a complicated multistage fabrication process can result in structure misalignment, higher risk of other defects, and reduced overall quality, nullifying the effects of microstructures inside the channel. Therefore, this work aims to additively manufacture hydrophilic microstructures directly inside microfluidic channels through the 2PP process for use in complex single body parts, avoiding extra assembly and post-processing. This allows for significantly higher customization and flexibility in the designed and manufactured part. Additionally, the design of the microstructure can be varied significantly, since there are minimal constraints for the shape design, other than the 2PP equipment's resolution. To demonstrate the capability of the technology in this paper, fractal hydrophilic microstructures (Figure 1b3 and c3) are selected for the variability in feature size, presence of multiple overhanging elements, manufacturing complexity, and high hydrophilic performance, which has been demonstrated for several

fractal microstructures on flat surfaces.[21] The capability to produce complex parts with microstructured channels is of great importance to numerous potential applications. One such hydrophilic microstructure application is its use in microfluidic channels to facilitate better flow performance and efficacy. Moreover, it has been reported that hydrophilic microstructures provide self-cleaning capabilities to microfluidic channels,[33] and can assist in filling complex or deeply embedded channels while reducing voids and defects.[31,34] However, work done on these topics has been mostly limited to parts printed in separate pieces and assembled afterward, hindering the structures' true potential.

Lastly, while a simple method to implement wetting morphologies on complex structures is developed and shown in this paper, there exist numerous notable applications of this technology that can be effectively implemented through the 2PP process. One of these applications includes anti-fouling coatings, where hydrophilic surfaces are used to retain a thin layer of water present on structures submerged in water for extended periods of time. This layer prevents the direct attachment of organisms and biological matter to the structure, which drastically reduces the amount of fouling possible.[35-37] The fabrication of low friction surfaces is a notable application of hydrophilic morphology, especially when exposed to water or a water-soluble solution, that is particularly useful in medical fields.[37-39] Another application utilizes hydrophilic coatings to separate and filter mixtures of oil, water, and other contaminants. Hydrophilic coatings can improve optical performance in lenses. Evenly spreading water over a lens forms a pseudo-lens, which prevents water droplets from accumulating on a flat lens, refracting light, and disturbing optical clarity.[37,40] Finally, when combined with hydrophobic microstructures, a hydrophilic coating is able to separate water-oil mixtures and clean contaminants from the water.[37,40,41] Hydrophobic microstructures share many applications with hydrophilic morphologies, such as anti-fouling and self-cleaning, but achieve them by repelling liquid and avoiding prolonged contact between the surface, the liquid, and its inclusions.[9] Moreover, hydrophobic microstructures stand out in the application of anti-icing and anti-corrosion that are critically important for a number of current technologies in energy and transportation.[42,43]

2. Materials & Methods

2.1. Materials:

- 2PP resins: IP-S and IP-Q (Nanoscribe GmbH, Eggenstein-Leopoldshafen, Germany) resins are used for 3D printing structures with hydrophobic and hydrophilic microstructures, respectively. Different materials are used solely due to the different size scales of the microstructures and utilized printing lenses.
- Propylene glycol monomethyl ether acetate (PGMEA) with 99.5% concentration (Sigma-Aldrich Co., St. Louis, MO, USA, part #484431) is used to develop 2PP printed IP-S and IP-Q parts.
- A surfactant-free 1.1 wt.% aqueous solution of an intrinsically conductive polymer poly(3,4-ethylenedioxythiophene)poly(styrenesulfonate) (PEDOT:PSS) (MilliporeSigma, Burlington, MA, USA, part #739332) is used for both the dipping process and filling the microstructured hydrophilic channels as an example of conductive solution for electrode coating due to its great application in various areas and the variety of commercially available aqueous solutions. The high content of water and absence of surfactants result in a water-like wetting behavior of the PEDOT:PSS solution, which simplifies its analysis and use with hydrophobic and hydrophilic structures.
- A 1.3 wt.% aqueous solution of an intrinsically conductive polymer PEDOT:PSS with 5% surfactant (MilliporeSigma, Burlington, MA, USA, part #483095) is used for some tests with hydrophilic microstructures to evaluate their interaction with fluids possessing lower surface tension.
- Surfactant plasticizer Triton X-100 ($C_{14}H_{22}O(C_2H_4O)_n$, where n=9-10) (Sigma-Aldrich Co., St. Louis, MO, USA, part #T8787) is added to PEDOT:PSS solution when electrode is used for the strain gauge experiment to reduce sensitivity of conductivity to low strains expected in the experiment and boost overall conductivity.[44] The materials are mixed such that the composition of the final electrode contained 20 wt.% PEDOT:PSS and 80 wt.% Triton X-100.

- Isopropanol (IPA) (Duda Energy LLC, Decatur, AL, USA, part #isoprop), 99.9% purity, is used for cleaning substrates, developing printed parts, and capillary testing of the microstructured hydrophilic channels due to its low surface tension.
- Acetone (Duda Energy LLC, Decatur, AL, USA, part #acetone2), 99.5% purity, is used for cleaning substrates before printing.
- Polydimethylsiloxane (PDMS), Sylgard 184 (Dow Inc., Midland, MI, USA, part #4019862) is used for testing the microstructured hydrophilic channels.

2.2. Two-Photon Polymerization Additive Manufacturing

The fabrication of the hydrophobic and hydrophilic microstructures, along with the channels, is accomplished using a Nanoscribe Photonic Professional GT2 system (Nanoscribe GmbH, Eggenstein-Leopoldshafen, Germany) that is equipped with a 780 nm laser with a pulse duration between 80-100 fs and a repetition rate of 80 MHz. Hydrophobic structures are printed with IP-S, a highly viscous 2PP curable resin. All prints using IP-S resin utilize the 25x objective (0.8 numerical aperture) lens along with 1 inch x 1 inch indium tin oxide (ITO) coated soda lime glass substrates (MSE Supplies, Tucson, AZ, USA). For this configuration (25x, IP-S, ITO glass), standard printing parameters of 50 mW output power, 1.0 power scaling, slicing distances of 1 μm, hatching distance of 0.5 μm, galvo speed of 100 mm s^{-1}, and stitching angles equal to or greater than 15° are used to maintain mushrooms with no stitching affects. For better data and visuals, some of the parts are printed near the edge of the ITO coated glass substrates, while others are printed in the center of the substrates. The hydrophobic channels are printed with IP-Q resin on 1 inch x 1 inch silicon substrates utilizing the 10x objective (0.4 numerical aperture) lens. Standard printing parameters used for this configuration (10x, IP-Q, silicon substrate) are 45 mW output power, 1.0 power scaling, slicing distances of 5 μm, hatching distances of 1 μm, and stitching angle of 15°.

All printed parts, with the exception of the channels, are developed in PGMEA for 20 minutes, then in IPA for 5 minutes, and are blown dry with an airball. Due to the microchannels being filled with liquid resin during printing, to ensure the channels are fully developed, they are placed in PGMEA for 1 hour at 70 °C, and then are placed in IPA for 10 minutes at 50 °C. The channels are then blown dry with an airball. The channels that appear to need more development are placed back in IPA and into a vacuum chamber set to 20 torr absolute pressure for less than a minute, to remove the air inside the channels while filling them with IPA. The parts are pulled out and left to sit in IPA for 10 minutes, and then are blown dry and inspected. If more development time is necessary, this process is repeated, applying sonication when needed.

2.3. Nanoindentation

Nanoindentation is performed to measure indentation hardness, H, and reduced modulus, E_r, later converted to Young's modulus, of the IP-S and IP-Q polymers using a Bruker Hysitron TI-980 TriboIndenter (Billercia, MA, USA). A force of 5 mN is applied to 300 μm diameter and 100 μm height cylindrical samples of IP-S and IP-Q with a 100 nm radius Berkovich diamond indenter prober. The measured reduced modulus and Poisson's ratio of 0.3 are used to calculate the Young's modulus of both the IP-S and IP-Q samples. Three segment indentation processes, including loading, unloading (1 mN s^{-1}), and a 5 sec dwell time, are executed as shown in Figure S1 (Supporting Information). The measured values for both IP-Q and IP-S are listed in Table S1 (Supporting Information).

2.4. Microscopy and Profilometry

A Filmetrics Profilm3D (KLA Corporation, Milpitas, CA, USA), an optical profilometer with 10x and 50x Nikon objectives, is used to measure the thickness distribution of the deposited electrode. In addition, a scanning electron microscope (SEM), the FEI Quanta 650 (Field Electron and Ion Company, Hillsboro, OR, USA), is used to assess the quality of the printed parts, and to investigate printing defects that could cause undesired wettability. The accelerating voltage of 10 kV is used for all the images.

3. Results & Discussions

3.1. Electrode Micropatterning

This section presents the design of 3D printed reentrant hydrophobic microstructures, its testing results, and its application for an AM microsize strain gauge by controlling surface wettability to pattern electrodes.

3.1.1. Design of Reentrant Hydrophobic Microstructure

Hydrophobic behavior of reentrant microstructures, such as a mushroom-like design with a cylindrical stem and cap, on horizontal flat surfaces is a well-established phenomenon.[2,8] Maintaining spacing of the microstructures to be less than a liquid's capillary length allows the liquid to be suspended, as shown in **Figure 2**a. Specifically, the liquid wets the top and side surfaces of the cap and remains suspended between the edges of the mushroom-design by its surface tension, γ, forming a suspended contact angle, θ , that varies due to the pressure difference, Δp, between the liquid and gas. If the pressure difference or the microstructure spacing is increased, the suspended contact angle would increase as shown in Figure 2b. When the suspended contact angle reaches the Young's contact angle, θ_Y, of the liquid on the microstructure material, liquid propagates along the cap's bottom surface and stems to the base surface, transitioning from Cassie-Baxter to Wenzel wetting state as depicted in Figure 2(c and d), respectively. As illustrated in Figure 2e, the liquid is supported by rectangular patterned microstructures while dipping. The sustained pressure can be obtained from the balance between the forces due to the external pressure and due to the surface tension at liquid-solid edges. The maximum pressure threshold can be approximated with Equation (1) when the suspended contact angle, θ, reaches the Young's contact angle, θ_Y;

$$\Delta p = p_L + p_h + p_p = \frac{\gamma \sin\theta \, \pi D}{\alpha^2 - \frac{\pi D^2}{4}} \tag{1}$$

where p_L is Laplace pressure, which is significant for small droplets, but has much smaller contribution when a liquid is spread more uniformly over a microstructured part during dipping; p_h is hydrostatic pressure, due to the depth of liquid, d_h, exerted on microstructures during dipping; p_p is perturbation pressure due to mechanical excitations of the microstructured part that are translated through the dipping apparatus and dynamic changes in environmental atmospheric pressure, etc.; D is cap diameter; α is the center-to-center spacing of the stems in a rectangular pattern.

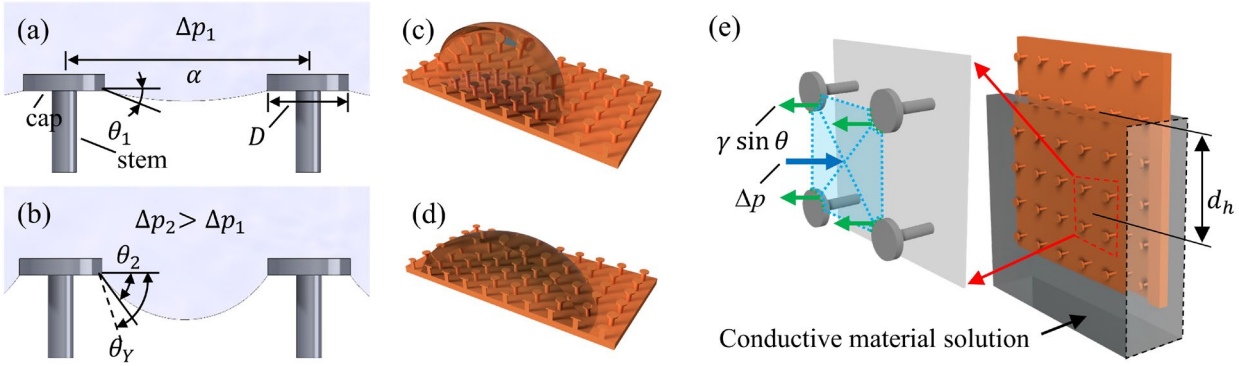

Figure 2. Principle of reentrant hydrophobic microstructures (a) suspending a liquid at low pressure difference and (b) a higher pressure difference; (c) Cassie-Baxter and (d) Wenzel wetting states of liquid on a microstructured surface; (e) pressure equilibrium principle during the dipping process of a part with reentrant hydrophobic microstructures.

For the successful implementation of the dipping process, several other factors need to be considered. In particular, a minimum residual amount of electrode material should remain on the hydrophobic microstructures. Therefore, liquid droplets should roll off the surface upon the dipping of a microstructured part. While predicting hysteresis is complicated, a simple estimate of wettability can be obtained from Cassie-Baxter model that describes liquid's apparent angle, θ^*, as shown in Equation (2).

$$\cos\theta^* = f_s \cos\theta_Y - f_g \quad (2)$$

where f_s is the solid fraction of contact with the liquid, i.e., the ratio of microstructures area in contact with the liquid to the projected area of the liquid-gas-microstructure contact, f_g is the gas fraction of contact with the liquid, i.e., the ratio of gas-liquid interface surface area to the projected area of the liquid-gas-microstructure contact. Because both horizontal and vertical surfaces of the reentrant microstructures wetted by the liquid and liquid-gas interface is curved between microstructures, the sum of solid and gas fractions are generally more than one, $f_s + f_g > 1$. Finally, θ_Y is the Young's contact angle between the liquid and the microstructures.[8] The usefulness of this relation for the developed dipping process lies in suggesting that the reentrant microstructures must result in a small solid fraction, f_s, to facilitate liquid droplets rolling off the microstructured surface after dipping. The relation between the solid fraction, f_s, Young's and apparent contact angles as per Equation (2) is illustrated well in literature.[8]

Furthermore, when liquid droplets do not completely roll off the surface, the effects of evaporation and consequent wetting must be considered. The transition from the Cassie-Baxter state to the Wenzel state during the droplet evaporation on horizontal microstructured hydrophobic surfaces has been studied with most common liquids, including water.[27,28] As the liquid evaporates, the droplet size decreases and is supported by a smaller number of structures until it 'slides' between the structures (transitioning to the Wenzel mode), leaving residues on hydrophobic structures and on the base surface where the wetting state transition occurs. Hence, similar experimentation with a solution of a conductive material would eventually result in a small conductive area on the base surface and multiple conductive structures. Therefore, the developed dipping technique must ensure that as little residue material is left on the hydrophobic region as possible to obtain high quality electrode patterning. To achieve that, the conductive solution must be supported by the hydrophobic microstructures and possess small wetting hysteresis on top of the hydrophobic morphology. Both tasks can be accomplished by adjusting the geometry of the structures and their surface quality.[45,46]

Numerous experimental studies on reentrant hydrophobic microstructures show that these structures typically have morphology dimensions of the same magnitude, often ranging between 20 µm and 90 µm. They can be manufactured using various microfabrication techniques and have demonstrated the ability to repel most commonly tested liquids.[8,14-16,19,22,27] For a simple mushroom-like reentrant microstructure that consists of a circular stem and circular disk-like cap, the average dimensions across literature are demonstrated in **Figure 3**a. However, when the microstructures are used for patterning electrodes during the fabrication of a micro- or mesoscale device, it is ideal to minimize their effect on the device's geometry and functionality, which can be achieved by reducing the microstructure's size. Moreover, previous studies have reported the greater performance of smaller-scale microstructures.[45,47] Meanwhile, there are several challenges to minimizing the size of reentrant hydrophobic microstructures. The first limitation is directly related to manufacturing pillared structures at a small scale due to their size and fragility. Secondly, there is a strict baseline requirement on the reentrant hydrophobic structures' quality and pattern integrity. Particularly, the failure of a single reentrant hydrophobic microstructure can lead to a complete failure of the hydrophobic layer due to liquid touching the base surface locally first and then propagating throughout the entire surface. AM of such miniaturized reentrant structures through the 2PP technique addresses both problems by enabling small-scale, high-quality features and replacing subtractive manufacturing with the additive process with its considerably lower chance of damaging the parts during fabrication. Therefore, the reentrant structure design is 2PP printed in a typical scale, then reduced to 1/3, and 1/6 size as shown in Figure 3(a-c), to investigate and demonstrate the fabrication capabilities. Furthermore, the performance of these three designs, in terms of the maximum liquid pressure that the microstructure can withstand, and the resulting apparent contact angle of droplets during their roll off after dipping is calculated through Equations (1) and (2). These results are graphed in **Figure 4**, conforming with the previous observations of higher performance with smaller microstructures. For calculations, the apparent contact angle of 1.1 wt.% aqueous PEDOT:PSS solutions on IP-S 2PP printed flat surface is measured as 58.9°, as shown in Figure S2 and reported in Table S2 (Supporting Information). A water-like surface tension of 70 mN m^{-1} is used for the PEDOT:PSS solution as per literature.[48] Figure 3a demonstrates that the typical scale structures

with the largest dimensions are printed with high fidelity on both the horizontal and vertical surfaces. The 1/3 design shows some deviation in shape between structures printed on the horizontal and vertical surfaces, as shown in Figure 3b. The sizing of this design is selected close to the resolution of the 2PP printer 25x objective and, therefore, is modified by the software to enable successful manufacturing on horizontal and vertical surfaces with the 2PP printing voxel, which is an ellipsoidal shape with a high aspect ratio. Firstly, the cap height is increased in microstructures printed on the horizontal surface, but it only somewhat increases solid fraction, f_s, and corresponding apparent angle, θ^*. Secondly, the decreased stem height does not leave much space for the curved liquid-gas interface that can cause a liquid contact with the base surface before the Young's contact angle is reached on the microstructure. Thus, the stem height is increased for this design for all further prints. Thirdly, the bottom cap surface is not perpendicular to the stem anymore, which somewhat compromises the hydrophobic performance by increasing the actual contact angle. Nevertheless, it still possesses the geometry of a reentrant structure and can be used if miniaturization of the microstructures is required. Finally, the structures shown in Figure 3c are fabricated to identify the maximum capability of the objective and prove that the Figure 3b design is the smallest possible implementation of the reentrant structure. Further minimization of the structure is possible when using a higher resolution objective, e.g., 63x lens (1.4 numerical aperture); however, it drastically increases the printing time of larger parts covered with microstructure. Hence, the reentrant microstructure design shown in Figure 3b, but with increased stem height, is used for the rest of the fabricated and tested parts.

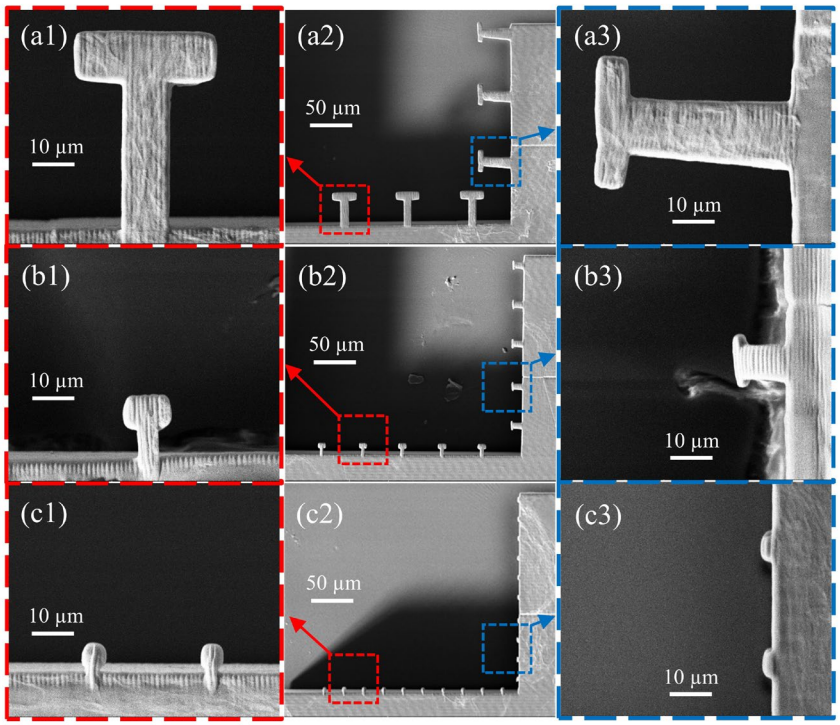

Figure 3. Scanning electron microscopy of the cross-sections of reentrant microstructures additively manufactured with Nanoscribe GT2 2PP printer: (a1-a3) common sizing across literature, (b1-b3) one-third minimized size, and (c1-c3) one-sixth minimized size.

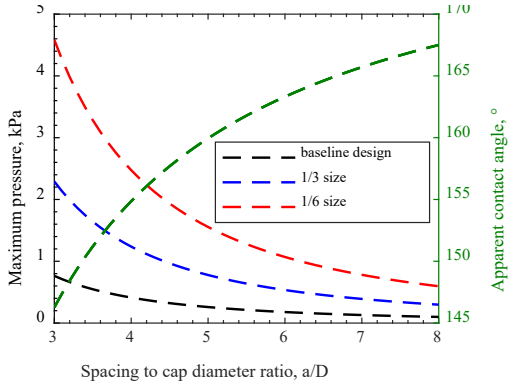

Figure 4. Performance of three hydrophobic microstructure designs 2PP printed with IP-S resin in terms of maximum liquid pressure and apparent contact angle with surfactant-free aqueous PEDOT:PSS solution (98.9 wt.% water). The baseline design represents the mushroom-like geometry with cap diameter of 30 µm and cap thickness of 6 µm. 1/3 and 1/6 size designs are proportionally miniaturized geometries, resulting in the same apparent contact angle for all three designs.

3.1.2. Wetting Morphology Integration for Selective Electrode Coating

This study aims to develop the wetting microstructure to pattern electrodes on parts of various geometries through the dipping process. Two samples with vertical and horizontal orientations of their base surfaces are first considered to investigate the wetting process during dipping. Testing setups, sample design features, and results are shown in **Figure 5** for the vertical and **Figure 6** for the horizontal samples. Both types of samples possess centrally located 0.5 mm x 0.5 mm areas intended to be coated with electrode material through the dipping process that can be seen in Figure 5a and Figure 6b. These areas are either left with no morphology or covered with cones to investigate the effect of hydrophilic morphology on the dipping process (Figure 5b1). The cones with equilateral triangle cross-sections and their sizing are selected to facilitate surface wetting and match the height of the hydrophobic structures. The remaining samples' area is covered with reentrant hydrophobic structures (Figure 5b3).

The final vertical sample design, demonstrated in Figure 5a, is further improved through experimentation and possesses a couple of modifications. The first vertical dip attempts demonstrated the inability of the utilized reentrant structures to support the liquid when it is fed sidewise to the microstructures. Therefore, vertical walls are added and further modified into inverted L-shapes to support the liquid on the edges of the hydrophilic region (Figure 5b4) and the whole vertical sample (Figure 5c), similarly to the individual reentrant structures. Lastly, Figure 5d shows the dipping setup for the vertical structure and Figure 5(e1-e3) demonstrates the sample right after dipping it once, after drying the first coated layer, and after drying the second coated layer. The PEDOT:PSS solution covers the hydrophilic area during the first dipping and also over the previously coated and dried layer. While successful coating is achieved, the dipping process unveils the importance of aligning the vertical structure with the PEDOT:PSS droplet to minimize the bending of the thin vertical structure and maintain correct wetting kinematics of microstructures. Furthermore, it is noticed that the vertical structures 2PP printed with IP-S bent less than samples made of IP-Q. This is attributed to the higher Young's modulus of IP-S polymer (3.396 ± 0.129 GPa) compared to the IP-Q polymer (1.488 ± 0.077 GPa), as measured with nanoindentation (Table S1 and Figure S1, Supporting Information).

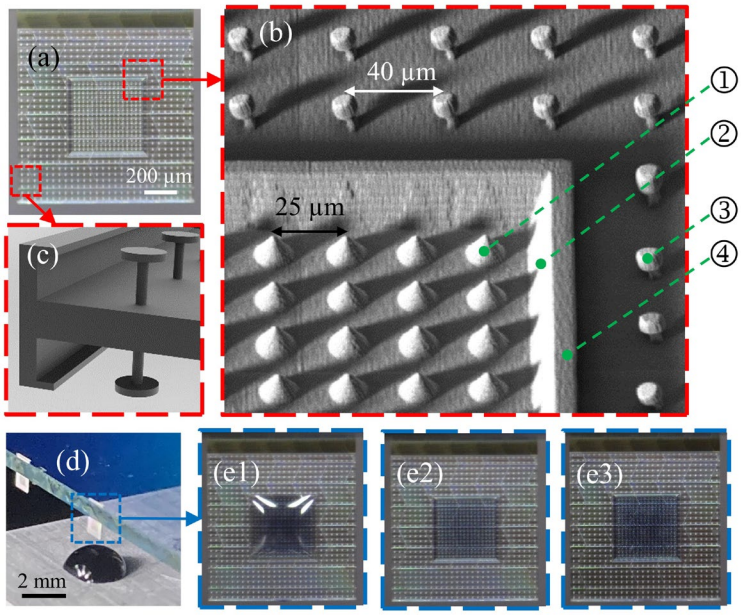

Figure 5. (a) Front view of a sample for the vertical dipping test. The design consists of inner 0.5 mm x 0.5 mm hydrophilic and outer hydrophobic areas. The microstructures include (b1) cones and (b2) the slope on the hydrophilic inner area, and (b3) hydrophobic reentrant structures (with the design as in Figure 3b) encircled by inverted L-shaped edges on the (b4) inner and (c) outer perimeters. (d) the vertical sample prepared for dipping in surfactant-free aqueous PEDOT:PSS solution (98.9 wt.% water) and its close-up view after (e1) dipping, (e2) drying first layer, and (e3) drying second layer, demonstrating electrode deposition of controlled thickness on preselected region.

Once the successful electrode coating through the dipping technique is achieved for the vertical sample, the dipping process is investigated on a horizontal sample with the same modifications as the vertical sample (Figure 6a). Two hydrophilic areas, with and without cones, are fabricated on the surface to quantify the effect of the hydrophilic microstructure on the horizontal sample (Figure 6b). First, the glass with the sample is placed above the PEDOT:PSS solution. Then, a substrate with the solution is raised until it touches most of the sample area (Figure 6c1). Figure 6c2 shows the horizontal sample right after the substrate with PEDOT:PSS solution is lowered. The hydrophilic area with cones attracts considerably more solution than the area without any morphology. When analyzed through profilometry, the average thicknesses of the cured electrodes are approximately 1.35 µm and 0.73 µm for the areas with and without cones, respectively (Figure 6d and Figure 6e).

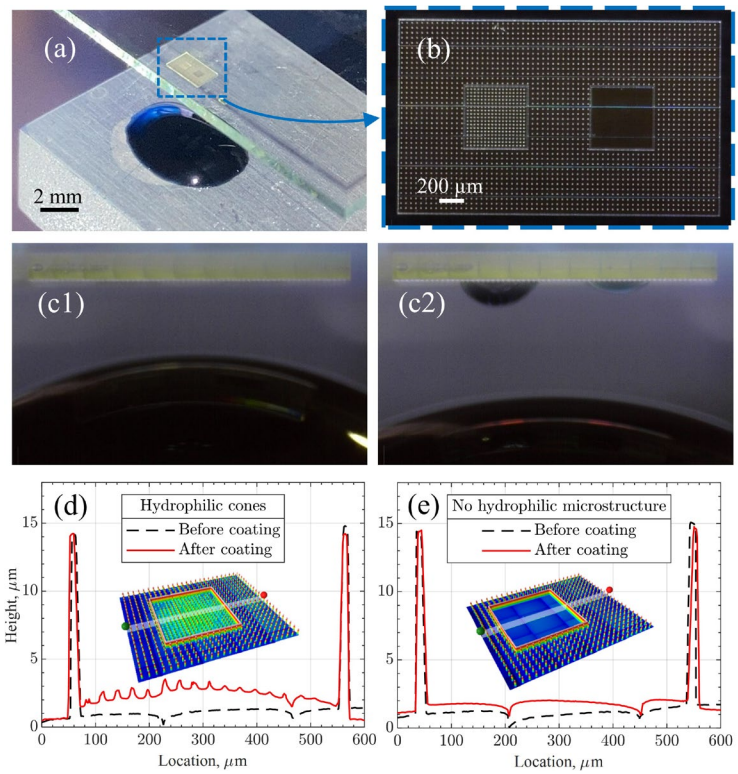

Figure 6. (a) Horizontal sample prepared for dipping in surfactant-free aqueous PEDOT:PSS solution (98.9 wt.% water) and (b) its close-up view. Two 0.5 mm x 0.5 mm hydrophilic areas with and without conical morphology are located in the center of the sample. Side view of the sample (c1) before and (c2) after the dipping demonstrating a larger amount of material grabbed by the conical morphology. The thickness of the dried PEDOT:PSS electrode deposited on hydrophilic areas (d) with and (e) without cones morphology.

3.1.3. Microsize Strain Gauge through Dipping

A microsize strain gauge with patterned electrode is fabricated through 2PP additive manufacturing and the developed dipping method, as shown in **Figure 7**a, to validate its ability to coat electrodes for functional structures. The device's design is adapted from a conventional linear film strain gauge. However, it operates in a cantilever mode to sense its deformation due to the applied stimulus and is scaled down to 1.37 mm in height. Its principle of operation is through the change of resistance in the electrode coated on the surface of the vertical 2PP printed IP-S structure. Similar to the typical strain gauge, two large electrode connections were also coated away from the main structure to connect with multimeter probes. When the cantilever strain gauge bends, the electrode on the surface undergoes either tension or compression, depending on the bending direction. This affects its cross-sectional area and length, subsequently influencing the resistance. Figure 7b shows the measured resistance gradually decreasing when up to 350 µm deflection is applied to

the cantilever strain gauge, as shown in the experimental setup in Figure 7c, which corresponds to about 0.8% strain in the coated electrode layer.

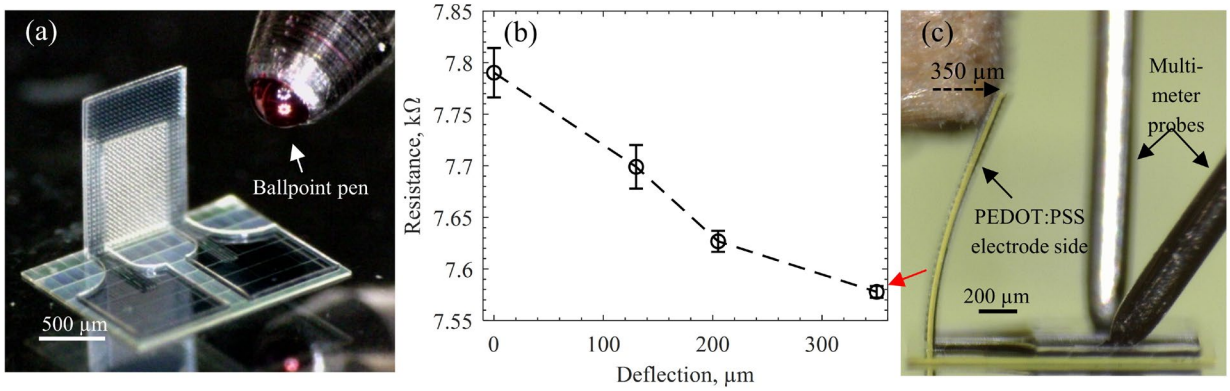

Figure 7. Testing sensing capabilities of (a) 2PP printed microsize cantilever strain gauge structure and electrode pattern coated through the dipping technique (b) gradually decreasing resistance as the electrode is compressed (c) when deflected up to 350 µm that corresponds to about 0.8% average strain in the coated PEDOT:PSS electrode at the root of the cantilever beam.

3.2. Enhanced Microchannel Filling

To study the effect of hydrophilic and hydrophobic microstructures in microscale channels, different microstructure patterns are designed and printed.

3.2.1. Microchannel Filling utilizing Hydrophilic Microstructures

The designed hydrophilic microstructures are cuboid and pyramid fractal shapes with four layers of geometric patterning that are 2PP printed with testing structures, as shown in **Figure 8**(a and b), respectively. A testing structure for measuring the change in capillary rise due to the effects of microstructure is also developed. A 4 mm long channel with a 3 mm diameter is patterned with microstructure, with a minimum feature size of 37.5 µm.

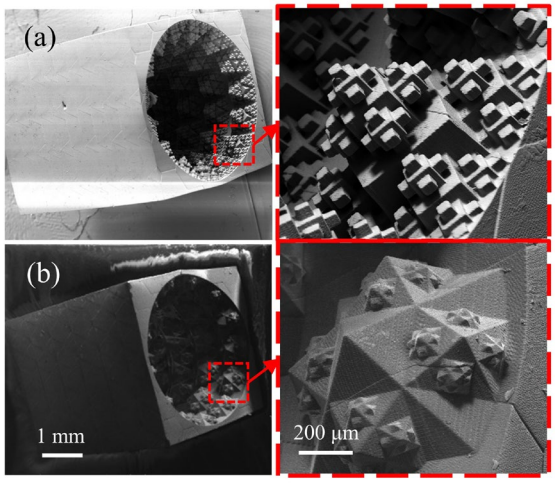

Figure 8. SEM imaging of the microstructured channels. (a) The cubic microstructure offers significantly more surface area than (b) the pyramid microstructure.

To determine the effect of the microstructure on the microchannel's wettability, an experiment is conducted to determine the change in capillary rise. For a cylindrical tube, the formula for capillary action is given by Equation (3).

$$h = \frac{2\gamma cos(\theta^*)}{\rho g r} \quad (3)$$

where h is the height of capillary rise, ρ is the fluid density, g is the gravity constant, and r is the radius of a cylindrical tube. Functionally, the addition of microstructure should minimally impact the surface tension of the liquid while drastically decreasing the contact angle, leading to an increase in the capillary rise. To determine this, microchannels are printed utilizing the 2PP printer, as described in Section 2.2. In addition to the patterned channels, a control channel is printed with no internal microstructure. The channels are then submerged in IPA fluid, and the depth of the meniscus is measured via microscopy, as shown in **Figure 9**. In general, IPA has a lower surface tension compared to other common materials (mostly water or aqueous solutions, such as PEDOT:PSS). This reduces the amount of capillary rise, as well as the size of the channel required for the experiment, which makes printing more efficient and practical.

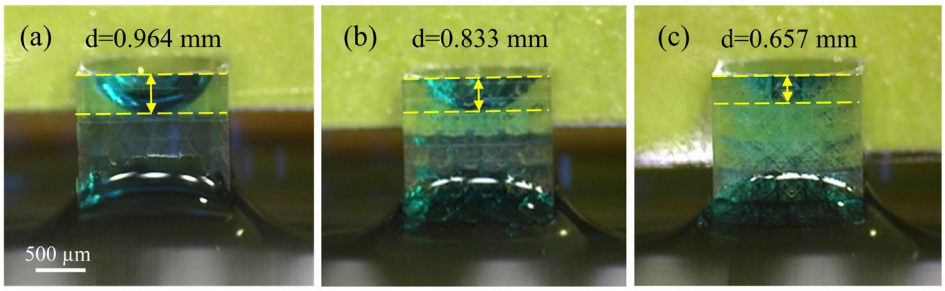

Figure 9. Meniscus depth inside (a) smooth, (b) pyramid, and (c) cubic channels when immersed in IPA, dyed blue to increase visibility.

In the capillary rise tests with IPA, the cubic microstructure demonstrates the highest hydrophilic effect, with a 10.1% increase in capillary effect over the smooth channel. The pyramid microstructure also shows an increase, although less pronounced, at 4.3%. Additionally, the effective contact angles for the IPA are calculated using the formula for capillary rise in a cylindrical channel using Equation (3), and are listed in **Table 1**. This results in a 7.4° decrease in contact angle with the addition of cubic microstructure, and a 3.0° decrease in contact angle with the pyramid microstructure. These results match the general observations and assumptions about the effects of hydrophilic microstructures.[21] The increase in surface area provides a greater adhesive force with the sidewall of the channels, allowing for a greater capillary rise.

Table 1. Testing results of IPA capillary rise in microstructured channels and calculated contact angles.

	Meniscus depth [mm]	**Capillary rise [mm]**	**Contact Angle**
Smooth	0.964	3.04	40.5°
Pyramid	0.833	3.17	37.5°
Cubic	0.657	3.34	33.1°

Finally, to test the efficacy of microstructures in retaining more viscous polymers like PDMS, a comparison is performed between the best performing structure-augmented channel and a smooth control channel. The tested channels are dipped into PDMS and allowed to fill via capillary action. The channels are then removed from the PDMS and allowed to drain, as shown in **Figure 10**. The efficacy of microstructured channels for that application is compared based on the height of the remaining fluid in the channels, h^*, measured after draining.

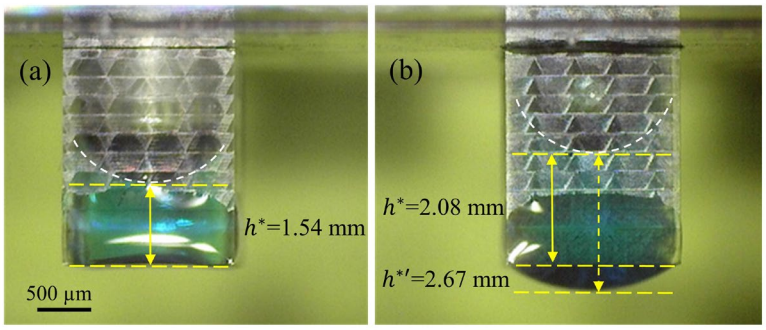

Figure 10. (a) Smooth and (b) cubic channels after being removed from PDMS and allowed to drain. The cubic channel retains significantly more PDMS than the smooth channel due to increased surface area.

The PDMS testing results are shown in **Table 2**. Similar to the IPA testing, the capillary rise of the PDMS is greater in the microstructured channel than in the smooth channel. Notably, when removed from the PDMS, the patterned channel retains a large amount of PDMS below the edge of the structure (h^{*}') that is still attached to the polymer initially pulled into the channel. This functionally increases the amount of PDMS present inside of the channel after the draining step, in comparison to the volume of polymer that flows into the channel via capillary action. However, the smooth control channel does not behave similarly, and loses a large portion of the PDMS after draining. This test underscores the advantages of microstructures in filling and retaining low surface tension, high viscosity fluids and polymers in microsize channels, making them valuable in sensor applications where very viscous polymers, especially when mixed with sensing dopants and other chemicals, are used.

Table 2. Testing results of capillary rise and retained height of PDMS in microstructured channels.

	Height [mm]	Height Retained [mm]
Smooth	1.83	1.54
Cubic	2.14	2.67 (2.08)

3.2.2. Selective Microchannel Filling utilizing Hydrophobic Inlet

One potential application of hydrophobic microstructures in structure-augmented microfluidic channels includes separating and filling specific channels independently. Below a certain size, microfluidics can easily move liquid throughout the entirety of a part. However, it can be desirable to have certain channels not filled with liquid or filled with a different liquid or polymer, such as for cooling, or mixing different sensing materials within a structure. **Figure 11**a demonstrates how a hydrophobic microstructure consisting of a circular wall with an inverted L-shaped cross-section can be added at the inlet hole of a channel to prevent the microchannel from filling until a certain liquid pressure is reached. The maximum pressure the hydrophobic inlet can withstand is obtained from the force balance as shown in Equation (4), when the contact angle, θ, approaches the Young's contact angle, θ_Y. Figure 11a relates the maximum pressure that can be withstood by the inlet to its diameter, when dipped in different liquids. Thus, the inlet can potentially be used to fill several channels with various, liquids controlled by the pressure that the hydrophobic microstructure is tailored to withstand. To experimentally demonstrate the design's effectiveness, a system of helical microfluidic channels with a diameter of 400 µm, one of which features the hydrophobic inlet with a diameter of 300 µm, is 2PP printed with IP-S resin and is demonstrated in Figure 11b. This system is then dipped into PEDOT:PSS solution to fill the channels. The regular inlet cannot resist the capillary effect, and the channel fills as depicted in Figure 11c. The inlet with the hydrophobic microstructure prevents liquid from entering the channel, and can serve as a venting channel. Furthermore, the hydrophobic microstructure is able to resist hydrostatic pressure up to the point when half of the structure (about 2 mm)

is dipped into the PEDOT:PSS solution. According to Equation (4), the printed design should withstand about 0.8 kPa of liquid pressure, which corresponds to the hydrostatic pressure at 8.15 mm depth of surfactant-free aqueous PEDOT:PSS solution. This suggests that dynamic perturbations during dipping might considerably contribute to the liquid pressure. However, the exact impact of perturbation is hard to evaluate, as hydrophobic performance is also affected by the quality of the printed structure, which is not optimized for this inlet.

$$\Delta p = \frac{\gamma \sin\theta \, \pi D}{\pi D^2/4} = \frac{4\gamma \sin\theta}{D} \tag{4}$$

where D is diameter of the hydrophobic inlet and the rest of variables same are as in Equation (1).

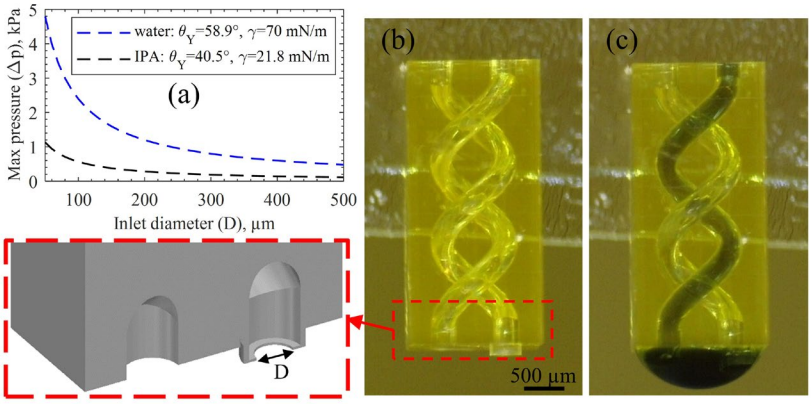

Figure 11. Hydrophobic inlet design for independent and controllable channel filling (400 µm channel diameter, 300 µm inlet diameter) with (a) maximum liquid pressure that it can withstand, i.e., pressure that needs to be applied to fill the channel with the inlet. A system of helical microchannels (b) before and (c) after immersion in surfactant-free aqueous PEDOT:PSS solution (98.9 wt.% water). One of the channels has a hydrophobic inlet preventing the solution from entering the channel.

4. Conclusion

This paper demonstrats successful electrode patterning, on-demand and enhanced microchannel filling utilizing 2PP AM, and the design of wetting morphologies. Primary and auxiliary hydrophobic and hydrophilic microstructures were designed and fabricated through the 2PP process on variously oriented external and internal surfaces, resulting in programmable wettability for electrode coating through the dipping technique. Analytical analysis estimated that liquid pressure on the order of several kPa that can be withstood by hydrophobic microstructures of a typical geometry, suggesting that dipping is not limited by hydrostatic pressure for the size of parts that can be manufactured through 2PP. The effectiveness of the method for electrode patterning was first studied on vertical and horizontal external surfaces by selectively coating microsize areas with the electrode material. It was then used to demonstrate fabrication simplicity with an example of a functional microsize strain gauge, tested in the cantiliever mode. The efficiency of the hydrophilic microchannels' morphologies was further evaluated by conducting the capillary rise test with various liquids. A new capability of the hydrophobic inlet was also designed and demonstrated for microchannels venting and selective filling. Future work of this study could focus on the design and fabrication of microsize devices that can drastically enhance their performance through the implementation of complex geometries and patterning methods enabled by 2PP and wetting morphologies.

Acknowledgements
This material is based upon work supported by the National Science Foundation under Grants No. 2018853 and No. 2229155. The opinions, findings, and conclusions, or recommendations expressed are those of the author(s) and do not necessarily reflect the views of the National Science Foundation.

References

[1] K. Koch, B. Bhushan, W. Barthlott, *Soft Matter* **2008**, 4, 1943.
[2] S. Parvate, P. Dixit, S. Chattopadhyay, *J. Phys. Chem. B* **2020**, 124, 1323.
[3] Z. Wang, M. Elimelech, S. Lin, *Environ. Sci. Technol.* **2016**, 50.
[4] X. Ye, Y. Li, Y. Zhang, P. Wang, *Journal of Bionic Engineering* **2022**, 19, 853.
[5] A. Tuteja, W. Choi, M. Ma, J. M. Mabry, S. A. Mazzella, G. C. Rutledge, G. H. McKinley, R. E. Cohen, *Science* **2007**, 318, 1618.
[6] N. J. Shirtcliffe, G. McHale, M. I. Newton, *Langmuir* **2009**, 25, 14121.
[7] J. M. Wigzell, R. C. Racovita, B. G. Stentiford, M. Wilson, M. T. Harris, I. W. Fletcher, D. P. K. Mosquin, D. Justice, S. K. Beaumont, R. Jetter, J. P. S. Badyal, *Colloids Surf., A* **2016**, 506, 344.
[8] T. L. Liu, C.-J. C. Kim, *Science* **2014**, 346, 1096.
[9] E. Arzt, H. Quan, R. M. McMeeking, R. Hensel, *Prog. Mater. Sci.* **2021**, 120, 100823.
[10] H. Ems, S. Ndao, *Appl. Surf. Sci.* **2015**, 339, 137.
[11] J. Zhou, D. A. Khodakov, A. V. Ellis, N. H. Voelcker, *Electrophoresis* **2012**, 33, 89.
[12] S. Banerjee, D. D. Dionysiou, S. C. Pillai, *Appl. Catal., B* **2015**, 176-177, 396.
[13] E. Gogolides, K. Ellinas, A. Tserepi, *Microelectron. Eng.* **2015**, 132, 135.
[14] R. Das, Z. Ahmad, J. Nauruzbayeva, H. Mishra, *Sci. Rep.* **2020**, 10, 7934.
[15] S. Hu, X. Cao, T. Reddyhoff, D. Puhan, S.-C. Vladescu, Q. Wang, X. Shi, Z. Peng, A. J. deMello, D. Dini, *ACS Appl. Mater. Interfaces* **2020**, 12, 4174.
[16] X. Liu, H. Gu, M. Wang, X. Du, B. Gao, A. Elbaz, L. Sun, J. Liao, P. Xiao, Z. Gu, *Adv. Mater.* **2018**, 30, 1800103.
[17] Y. Lin, R. Zhou, J. Xu, *Adv. Mater. Interfaces* **2018**, 5, 1801126.
[18] G. Graeber, O. B. Martin Kieliger, T. M. Schutzius, D. Poulikakos, *ACS Appl. Mater. Interfaces* **2018**, 10, 43275.
[19] X. Liu, H. Gu, H. Ding, X. Du, Z. He, L. Sun, J. Liao, P. Xiao, Z. Gu, *Small* **2019**, 15, 1902360.
[20] A. D. Lantada, S. Hengsbach, K. Bade, *Bioinspiration Biomimetics* **2017**, 12, 066004.
[21] E. Davis, Y. Liu, L. Jiang, Y. Lu, S. Ndao, *Appl. Surf. Sci.* **2017**, 392, 929.
[22] Z. Dong, M. F. Schumann, M. J. Hokkanen, B. Chang, A. Welle, Q. Zhou, R. H. A. Ras, Z. Xu, M. Wegener, P. A. Levkin, *Adv. Mater.* **2018**, 30, 1803890.
[23] S. Hu, X. Cao, T. Reddyhoff, D. Puhan, W. Huang, X. Shi, Z. Peng, D. Dini, *ACS Appl. Mater. Interfaces* **2019**, 11, 20528.
[24] A. Ruggiero, V. Criscuolo, S. Grasselli, U. Bruno, C. Ausilio, C. L. Bovio, O. Bettucci, F. Santoro, *Chem. Commun. (Cambridge, U. K.)* **2022**, 58, 9790.
[25] T. Stark, S. Sikulskyi, R. Srinivasaraghavan Govindarajan, D. Kim, in *SPIE Smart Structures + Nondestructive Evaluation*, Long Beach, CA, **2023**.
[26] T. Stark, D. Kim, in *SPIE Smart Structures + Nondestructive Evaluation*, Long Beach, CA, **2023**.
[27] X. Chen, J. A. Weibel, S. V. Garimella, *Sci. Rep.* **2015**, 5, 17110.
[28] R. K. Annavarapu, S. Kim, M. Wang, A. J. Hart, H. Sojoudi, *Sci. Rep.* **2019**, 9, 405.
[29] A. Tony, I. Badea, C. Yang, Y. Liu, G. Wells, K. Wang, R. Yin, H. Zhang, W. Zhang, *Polymers* **2023**, 15, 1926.
[30] C.-T. Kung, H. Gao, C.-Y. Lee, Y.-N. Wang, W. Dong, C.-H. Ko, G. Wang, L.-M. Fu, *Chem. Eng. J.* **2020**, 399, 125748.
[31] X. Zhao, C. Ma, D. S. Park, S. A. Soper, M. C. Murphy, *Sens. and Actuators, B* **2022**, 361, 131687.
[32] D. Wu, S.-z. Wu, Q.-D. Chen, S. Zhao, H. Zhang, J. Jiao, J. A. Piersol, J.-N. Wang, H.-B. Sun, L. Jiang, *Lab Chip* **2011**, 11, 3873.
[33] S. Nundy, A. Ghosh, T. K. Mallick, *ACS Omega* **2020**, 5, 1033.
[34] M. Choi, Y. Na, S.-J. Kim, *Electrophoresis* **2015**, 36, 2896.
[35] I. Jiménez-Pardo, L. G. J. Van der Ven, R. A. T. M. Van Benthem, G. De With, A. C. C. Esteves, *Coatings* **2018**, 8, 184.

[36] D. Ariono, A. K. Wardani, *IOP Conf. Ser.: Mater. Sci. Eng.* **2017**, 214, 012014.
[37] D. Ahmad, I. van den Boogaert, J. Miller, R. Presswell, H. Jouhara, *Energy Sources, Part A* **2018**, 40, 2686.
[38] R. J. LaPorte, *Hydrophilic Polymer Coatings for Medical Devices: Structure/Properties, Development, Manufacture and Applications*, Taylor & Francis Group, New York **1997**.
[39] A. Niemczyk, M. El Fray, S. E. Franklin, *Tribol. Int.* **2015**, 89, 54.
[40] S. K. Sethi, G. Manik, *Polym.-Plast. Technol. Eng.* **2018**, 57, 1932.
[31] Z. Xue, Y. Cao, N. Liu, L. Feng, L. Jiang, *J. Mater. Chem. A* **2014**, 2, 2445.
[42] S. S. Latthe, R. S. Sutar, A. K. Bhosale, S. Nagappan, C.-S. Ha, K. K. Sadasivuni, S. Liu, R. Xing, *Prog. Org. Coat.* **2019**, 137, 105373.
[43] E. Vazirinasab, R. Jafari, G. Momen, *Surf. Coat. Technol.* **2018**, 341, 40.
[44] S. Sikulskyi, *Ph.D.*, *Embry-Riddle Aeronautical University* **2021**
[45] C. Dorrer, J. Rühe, *Beilstein J. Nanotechnol.* **2011**, 2, 327.
[46] A. Giacomello, L. Schimmele, S. Dietrich, *Proc. Natl. Acad. Sci. U. S. A.* **2016**, 113, E262.
[47] D. Zhang, H. Li, X. Chen, H. Qian, X. Li, *Adv. Mater. Sci. Eng.* **2014**, 2014, 342184.
[48] G. Liu, Y. Liu, M. Zhang, F. Pettersson, M. Toivakka, *Materials* **2020**, 13.